

## ENA detection in the dayside of Mars: ASPERA-3 NPD statistical study

A. Mura<sup>a,\*</sup>, S. Orsini<sup>a</sup>, A. Milillo<sup>a</sup>, E. Kallio<sup>b</sup>, A. Galli<sup>c</sup>, S. Barabash<sup>d</sup>, P. Wurzc,  
A. Grigoriev<sup>d</sup>, Y. Futaana<sup>d</sup>, H. Andersson<sup>d</sup>, R. Lundin<sup>d</sup>, M. Yamauchi<sup>d</sup>, M. Fraenz<sup>e</sup>,  
N. Krupp<sup>e</sup>, J. Woch<sup>e</sup>, K. Asamura<sup>f</sup>, A.J. Coates<sup>g</sup>, C.C. Curtis<sup>h</sup>, K.C. Hsieh<sup>h</sup>, B.R. Sandel<sup>h</sup>,  
A. Fedorov<sup>i</sup>, M. Grande<sup>j</sup>, H. Koskinen<sup>k</sup>, J.U. Kozyra<sup>l</sup>, J.G. Luhmann<sup>m</sup>, S. McKenna-  
Lawlor<sup>n</sup>, R. Cerulli-Irelli<sup>a</sup>, R. D'Amicis<sup>a</sup>, M. Maggi<sup>a</sup>, S. Massetti<sup>a</sup>, E.C. Roelof<sup>m</sup>, P.C. Brandt<sup>o</sup>,  
D.J. Winningham<sup>p</sup>, R.A. Frahm<sup>p</sup>, J.R. Sharber<sup>p</sup>

<sup>a</sup>*Instituto di Fisica dello Spazio Interplanetario, Rome, Italy*

<sup>b</sup>*Finnish Meteorological Institute, Helsinki, Finland*

<sup>c</sup>*Physikalisches Institut, University of Bern, Bern, Switzerland*

<sup>d</sup>*Swedish Institute of Space Physics, Kiruna, Sweden*

<sup>e</sup>*Max-Planck Institut fur Sonnensystemforschung, Katlenburg-Lindau, Germany*

<sup>f</sup>*Institute of Space and Astronautical Science, Sagamihara, Japan*

<sup>g</sup>*Mullard Space Science Laboratory, University College London, UK*

<sup>h</sup>*University of Arizona, Tucson, USA*

<sup>i</sup>*Centre d'Etude Spatiale des Rayonnements, Toulouse, France*

<sup>j</sup>*University of Wales, Aberystwyth, UK*

<sup>k</sup>*University of Helsinki, Helsinki, Finland*

<sup>l</sup>*Space Physics Research Laboratory, University of Michigan, Ann Arbor, USA*

<sup>m</sup>*Space Science Laboratory, University of California in Berkeley, Berkeley, USA*

<sup>n</sup>*Space Technology Ltd., National University of Ireland, Maynooth, Ireland*

<sup>o</sup>*Applied Physics Laboratory, Johns Hopkins University, Laurel, USA*

<sup>p</sup>*Southwest Research Institute, San Antonio, USA*

Accepted 8 August 2007

Available online 1 January 2008

---

### Abstract

The Analyzer of Space Plasma and Energetic Atoms (ASPERA-3) on board Mars Express is designed to study the interaction between the solar wind and the atmosphere of Mars and to characterize the plasma and neutral gas environment in near-Mars space. Neutral Particle Detectors (NPD-1 and 2), which form part of the ASPERA-3 instrument suite, are Energetic Neutral Atom (ENA) detectors which use the time-of-flight (ToF) technique to resolve the energy of detected particles. In the present study, we perform a statistical analysis of NPD ToF data collected between 14 March 2004 and 17 June 2004 when Mars Express was located at the dayside of Mars looking toward the planet. After pre-processing and removal of UV contamination, the ToF spectra were fitted with simple analytical functions so as to derive a set of parameters. The behavior of these parameters, as a function of spacecraft position and attitude, is compared with a model, which describes ENA generation by charge exchange between shocked solar wind protons and extended Martian exosphere. The observations and the model agree well, indicating that the recorded signals are charge-exchanged shocked solar wind.

© 2008 Elsevier Ltd. All rights reserved.

*Keywords:* ENA; Mars

---

\*Corresponding author. Fax: +39 064993 4383.

E-mail address: [alessandro.mura@ifsi-roma.inaf.it](mailto:alessandro.mura@ifsi-roma.inaf.it) (A. Mura).

## 1. Introduction

Energetic Neutral Atoms (ENAs) originate in the neutralization of energetic plasma by exospheric gasses. In this *charge-exchange* (CE) process, an incoming ion captures an electron from the ambient neutral gas. The newly formed ENA retains both the energy and direction of the ion. Since ENAs are not affected by electromagnetic fields, they travel along straight lines just like photons. Their detection is, thus, usually referred to as “ENA imaging”. This technique is a useful way to remotely and globally study the property of the source plasma (Roelof and Williams, 1988). The ESA mission Mars Express carries a plasma and neutral particle package named the Analyzer of Space Plasma and Energetic Atoms (ASPERA-3) (Barabash et al., 2004). The Neutral Particle Detectors (NPD), part of ASPERA-3, is a neutral mass analyzer, and can resolve particle velocities and masses with low angular resolution. Since the solar wind (SW) interacts with Mars mainly through direct impact with its ambient gas (Kallio et al., 1997), CE is expected to be very effective there. ENA imaging is, hence, a potentially useful tool to allow insight into the geometry, the physics, and the dynamics of the plasma around Mars.

Here we present a statistical study of NPD Time-of-Flight (ToF) data, collected on the dayside of Mars during 3 months of 2004. So far, at least two different ENA signals were detected, namely (1) ENA albedo, produced when ENAs are generated above the Induced Magnetosphere Boundary/IMB (Lundin et al., 2004), cross the IMB and are back-scattered against the exobase (Futaana et al., 2006a); and (2) ENA jets, i.e. spatially constrained and highly directional ENA fluxes up to  $7 \times 10^5 \text{ cm}^{-2} \text{ sr}^{-1} \text{ s}^{-1}$ , in the 0.3–3 keV range, emanating from a compact region of the sub-solar exosphere (Futaana et al., 2006b, Grigoriev et al., 2007).

## 2. Instrument and data set

NPD is a pinhole camera acting as a mass and energy spectrometer with raw angular resolution  $5^\circ \times 40^\circ$ , providing ToF measurement and mass resolution (Barabash et al., 2004). Two NPD units are included in ASPERA-3, pointing in different directions, with six sectors covering a global Field of View (FoV) of  $9^\circ \times 180^\circ$ . We analyzed the NPD data recorded by both units in the dayside of Mars in the time period 14 March 2004 to 17 June 2004, in BIN mode only (ToF data are binned into 16 log. channels). The mass resolution of NPD was not utilized since it was assumed that all particles are H (Galli et al., 2006); the data were “downsampled” to a time resolution of 30 s ( $\Delta T$ ) through integration (to decrease the inherent noise); for each  $\Delta T$ , a 16-channel ToF spectrum has been obtained. Using these ToF values, we calculated the energy-per-nucleon (for simplicity, in what follows, we will refer to this as the “energy”,  $E$ ), assuming a ToF path of 8 cm. The  $s/c$  was in “nadir” mode, and sectors 0 of NPD1 and NPD2

(NPD1-0 and NPD2-0) always pointed towards Mars. All other sectors, and especially those of the NPD2, were always pointing away from the sun. None was pointing completely away from the planetary environment (where the ENA flux is expected to be generated).

## 3. UV filtering

UV suppression in the NPD is based on the coating of the start surface (to minimize UV efficiency), the coincidence of the start/stop signals and selection of the stop surface coating and start/stop electron optics. Nevertheless, NPD is still sensitive to UV and several post-acquisition UV suppression methods have been proposed (Futaana et al., 2006b, Galli et al., 2007). Here, we assume that the highest ToF channel contains only UV counts and no real data. In fact, for  $H$ , this channel corresponds to  $E \cong 10 \text{ eV}$ , too low to be detected by the stop MCPs (for O,  $E \cong 200 \text{ eV}$ , so that counts could represent a real ENA signal). The UV count rate for all other ToF channels can be calculated in the following way. We assume that some photons cause false start and stop signals with frequencies (respectively)  $F$  and  $F^*$ , where  $F = kF^*$  and  $k \gg 1$ . The ToF ( $t$ ) distribution of these false events is:  $f(t) = Fe^{-Ft}$ . The total number of UV false counts per second is equal to  $F^*$ ; the number of UV false counts  $N_{ij}$  between  $t_i$  and  $t_j$  is:

$$N_{ij} = F^* \int_{t_i}^{t_j} Fe^{-Ft} dt = \frac{F}{k} (e^{-Ft_i} - e^{-Ft_j}). \quad (1)$$

To obtain  $F$  from this equation we calculate the Maclaurin expansion:

$$N_{ij} \cong -\frac{F^2}{k} (t_i - t_j) + \frac{F^3}{2k} (t_i^2 - t_j^2) + \dots \quad (2)$$

$k$  is usually around 30 (Futaana et al., 2006b), and is obtained from data headers. Here we have used the last channel ( $t_i = 1514 \text{ ns}$ ,  $t_j = 1900 \text{ ns}$ ) to obtain  $F$  from Eq. (2). Then we calculated  $N$  for the other channels and subtracted it from the (related) measured count rates. It is worth noting that, assuming only H-ENAs are present, it is safe also to use the last two or three channels ( $E < 40 \text{ eV}$ ). In fact, in a preliminary test, we used a similar procedure with the last three channels and obtained similar results. An example of data before and after the removal of UV contamination is shown in Fig. 1.

## 4. Data analysis

To determine the characteristics of the ENA spectra, we fitted every spectrum with the sum of a Gaussian function plus a constant threshold, which represents residual noise:

$$f(x) = \underbrace{A \exp\left(-\frac{(\ln(E) - p)^2}{2\sigma^2}\right)}_{\text{ENA}} + \underbrace{c}_{\text{noise}}, \quad (3)$$

where  $A$ ,  $p$ ,  $\sigma$ , and  $c$  are free parameters. To preserve the original statistical weight of the count rate of each channel,

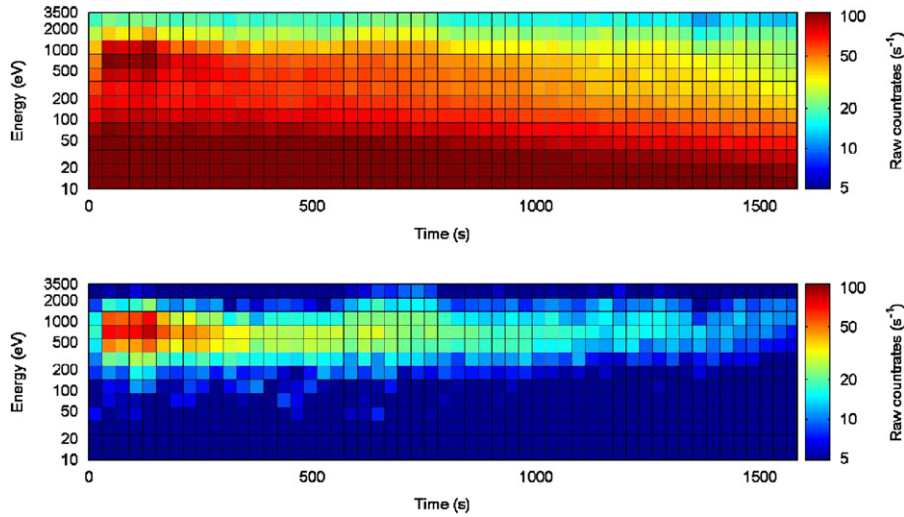


Fig. 1. Example NPD1-2 data, in an energy vs. time frame. Top: raw counts; bottom: after UV removal. Time is in seconds from May 28, 2004, 11:47:43 h.

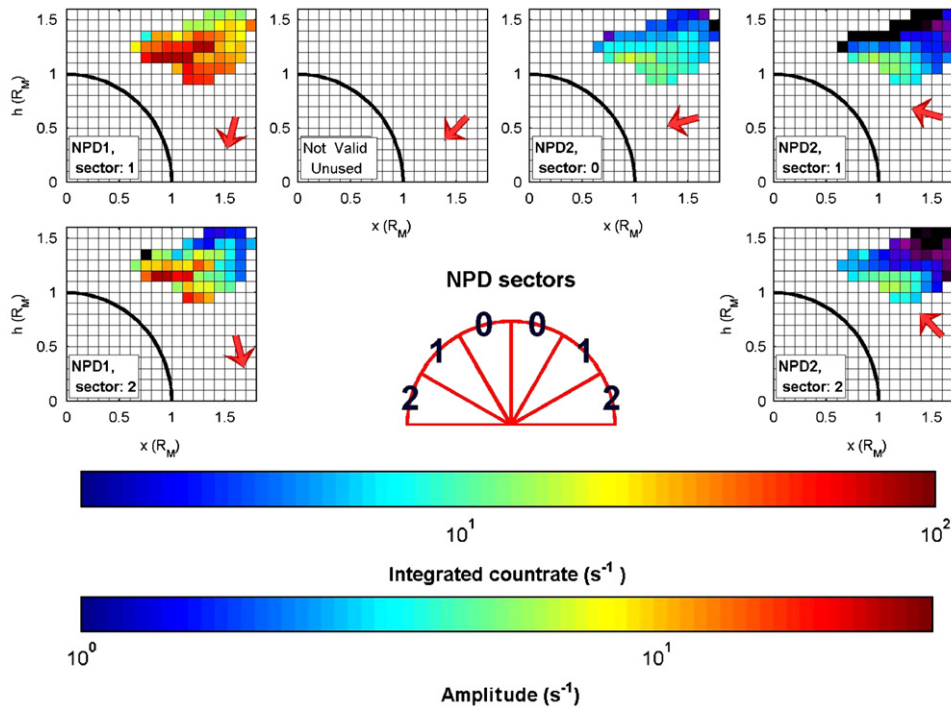


Fig. 2. Pseudo-color maps, in cylindrical coordinates, of the integral  $I$ . The color is coded according to the mean value inside a cell of  $0.1 \times 0.1$  (in Mars' radii). White cells have no statistical coverage. Red arrows represent, approximately, the central direction of each sector's FoV. The amplitude  $A$  is approximately proportional to  $I$  and can be deduced from the bottom color bar.

we applied this procedure directly to the UV-filtered data  $N$ . Then we deduced the energy spectra  $F(E) = f/\Delta E$  and the ToF spectra  $F(t) = f/\Delta t$  (see Appendix for details). We decided to discard all those spectra that looked “suspect” in any way (for example, those spectra where a single channel displayed an unreasonably high value). The total number of spectra to be processed ( $S$ ) after this phase, was  $\sim 10^4$ . NPD1-0 failed in early stage and has poor statistics. Thus, its data have been excluded. The spatial statistical

coverage of the valid data can be deduced from Fig. 2; most of the data were collected at a planetocentric distance ( $r$ ) between 1.5 and 2 Mars' radii ( $R_M \sim 3400$  km) and at a solar zenith angle ( $\alpha$ ) from the Sub-Solar Point (SSP) between  $40^\circ$  and  $70^\circ$ . After the best-fit procedure (least squares method), we obtained an array of  $S$  values for  $A$ ,  $p$ ,  $\sigma$ , and  $c$ . We also calculated the integrated count-rate between 350 eV and 3.5 keV ( $I$ ), by integrating the Gaussian function only. Due to the absence of an intrinsic,

global magnetic field (Acuna et al., 1998), we can assume, to a first approximation, that the plasma flows around the planet, and hence the ENA distribution, displays cylindrical symmetry, assuming that the possible influence of the IMF is smoothed out in our statistical study. Hence, we have defined a cylindrical coordinate system: ( $x$  from Mars' center to Sun;  $h$  perpendicular to  $x$ ), with a resolution of  $0.1R_M$ . Taking into account the average  $s/c$  velocity,  $\Delta T$  corresponds to less than 100 km. Hence, the temporal integration does not affect our spatial resolution significantly. Next, we calculated the mean value of each parameter within each grid cell. In Fig. 2 we show the results from this procedure in terms of  $I$  and  $A$ . The width  $\sigma$  is approximately uniform and around 0.8;  $p$  is between 0.5 and 1 keV (where  $A$  is relevant).

## 5. Interpretation of data

Even though the sector count rates are not inter-calibrated, it is possible to assume, as a zero-order hypothesis, that the relative count rates reflect the relative incoming flux. Under this assumption, the detected flux is higher in NPD1-1 and -2, which look towards the SSP. The amplitude  $A$  is up to  $20 \text{ s}^{-1}$  and is inversely proportional to  $r$ ;  $p$  is approximately uniform in space and between 500 eV and 1 keV. By applying Eq. (5) we can estimate that, on average, the  $E$  spectra peak around 500 eV, while the ToF spectra peak around 200 ns. If we consider NPD1-1,  $A$  decreases with increasing distance ( $r$ ) from  $\sim 20 \text{ s}^{-1}$  at  $1.5R_M$  to below  $10 \text{ s}^{-1}$  at  $2R_M$ . On the other hand, there is no evident correlation with the angle  $\alpha$ . Hence, these observations are consistent with an ENA source located close to the dayside planetary surface and emitting a radial flux (from the source). Assuming such a source, NPD1-2 points towards this ENA generation region only when the  $s/c$  distance  $r$  is small (i.e.  $\sim 1.5R_M$ ). In fact, the decrease of  $A$  vs.  $r$  is more pronounced. Moreover, the overall flux is high for sectors NPD1-1 and NPD1-2, since they point approximately counter to the direction of the expected ENA flux, while the flux is small for NPD2, which looks away from the generation region.

To investigate the hypothesis that the CE of shocked SW protons with the exosphere (Holmström et al., 2002) generates the features observed, we performed a simulation of the expected signal using an ENA simulation model (Mura et al., 2002). This model uses an analytical description of the  $\text{H}^+$  flow around the planet (velocity, density and temperature; Kallio, 1996) and the exospheric profiles of H,  $\text{H}_2$ , and O (Krasnopolsky and Gladstone, 1996). To take into account recent observations of smaller exospheric profiles (Galli et al., 2007), we reduced them by a factor of 10. The model predicts a maximum production of ENA ( $d\Phi/dx$ , generated flux per unitary length) on the dayside below the bow shock; by using an unperturbed solar wind velocity of  $4 \times 10^5 \text{ m s}^{-1}$  and density of  $2.5 \text{ cm}^{-3}$ , we obtain that  $d\Phi/dx$  is of the order of  $1 \text{ cm}^{-2} \text{ s}^{-1} \text{ m}^{-1}$ .

For each sector and for each of the  $S$  spectra, we computed the simulated ENA signal between 0.3 and 3 keV, taking into account the real  $s/c$  position and NPD attitude and using *line of sight* integration. Then we estimated the detected flux for NPD, in the same energy range, using the geometrical factor ( $5 \times 10^{-5} \text{ cm}^2 \text{ sr}$ ; Grigoriev et al., 2003) and  $I$ . In Fig. 3 we show the distribution of the detected integrated flux (panel A), for all sectors together, as a function of the angle  $\beta$  between the FoV direction and a point  $P$  located at  $(1.2, 0, 0) R_M$  ( $x$ -axis), and of the distance from  $P$  ( $y$ -axis). The distribution of the simulated flux is shown in panel B. The bulk of the signal is for  $\beta < 50^\circ$  in both panels. The point  $P$  is chosen in order to roughly represent an ENA source region located on the dayside of the planet, close to the surface (of course, the actual source is not restricted to a point). The position of  $P$  is arbitrary within a certain range: we have found that results similar to those shown in Fig. 3 can be obtained by locating  $P$  anywhere between  $1.1$  and  $1.5R_M$ , i.e. there is in this range general agreement between the experimental values (panel A) and the simulated values (panel B). This uncertainty could also be due to the wide angular resolution of NPD. The observations and the simulation differ when the angle from SSP is larger than  $50^\circ$ . In this case, the simulated flux is close to zero, while the observed flux (mostly for NPD-2) decreases with increasing distance. The observations and the simulation differ when the angle from SSP is larger than  $50^\circ$ . In this case, the simulated flux is close to zero, while the observed flux (mostly for NPD-2) decreases with increasing distance. This may be related to: (1) residual signal contamination (see Fig. 2, NPD-2); (2) plasma boundaries thickness, which is infinitesimal in model and finite in reality; (3) plasma boundaries variability during the 3 months of observation time; (4) the presence of another ENA production process not included in the model.

We considered the possibility of data contamination due to “pseudo-ENAs”, coming from the neutralization of ions in the entrance system. Such ENAs may have been observed, for example, by the replica instrument ASPERA-4 NPD on board Venus Express during the cruise phase to Venus (A. Galli and M. Fraenz, private communication). However, they have not been observed under similar circumstances, or during calibrations, by ASPERA-3 NPD. Moreover, such a contamination, if present, should be higher in NPD1-2 (see Fig. 2), which points approximately counter to the plasma flux direction in the observation region, while the data show a maximum in NPD1-1. The possibility of a residual, partial UV contamination should be considered as well. However, it should be noted that:

- (1) UV cannot produce a peak in the ToF spectrum.
- (2) The average values of the count rates agree with the estimations (Fig. 3, panels A and B)

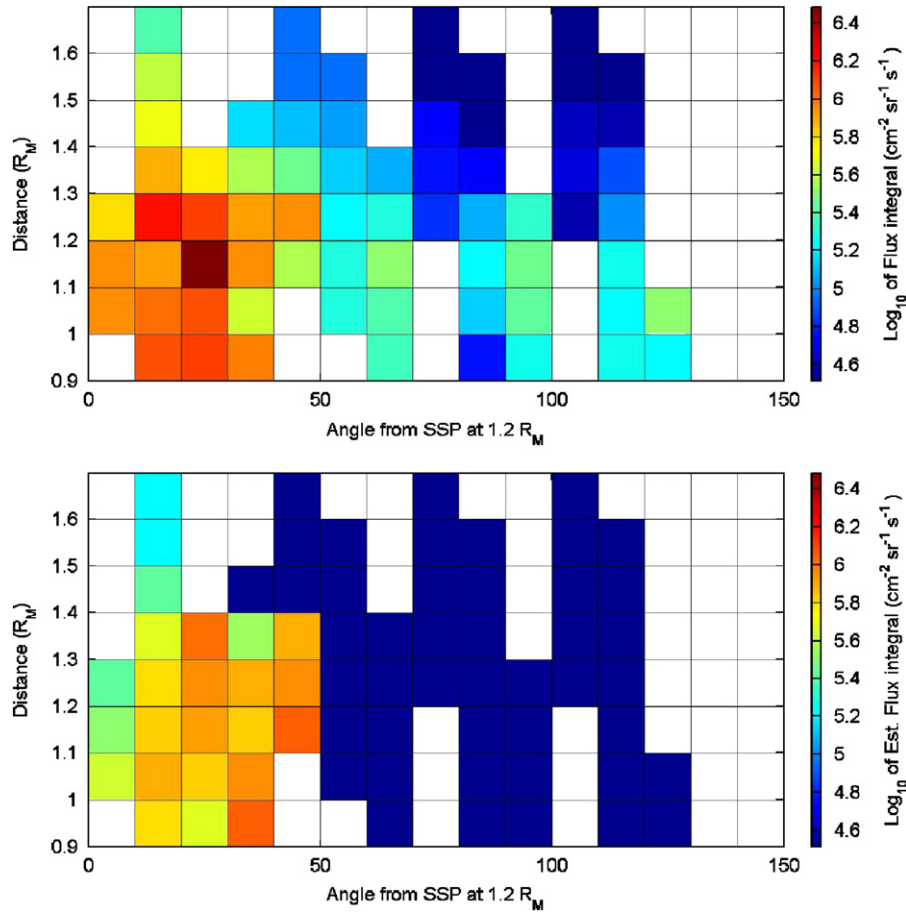


Fig. 3. (A) Pseudo-color map of the integral flux, as a function of the angle  $\beta$  between the FoV direction and the point P (1.2, 0, 0  $R_M$ ) ( $x$ -axis), and of the distance from P ( $y$ -axis). (B) Simulation (see text for more details).

## 6. Concluding remarks

In summary, the analysis technique described here is able to give a spatial and energy characterization of the ENA signal detected by ASPERA-3 NPD on the dayside of Mars. We have shown that this signal is in good agreement with theoretical predictions, assuming a signal coming from CE in the SW downstream of the bow shock. The detected flux may be up to  $10^6 \text{ cm}^{-2} \text{ sr}^{-1} \text{ s}^{-1}$ .

The main limitation of the study is the limited data period covered. This will be addressed, in the future, by extending the time period to include all the available data. Moreover, in this study we used, as a zero order hypothesis, constant calibration factors whereas it is in fact expected that these factors differ slightly from sector to sector, and are not constant with respect to ENA energy. This causes some systematic error in the determination of the peak energy ( $p$ ). In future work, the use of an energy-dependent calibration constant will allow a better energy description of the detected signal to be achieved. Finally, in our ENA model we excluded at least one possible candidate for ENA production (ENA albedo). Including more generation processes may probably help to explain remaining discrepancies between the measured data and the simulations.

## Acknowledgments

ASI supported IFSI contribution under contract N386. NASA supported US contribution under contract NASW 0003.

## Appendix

Here we define  $x = \ln(E)$ , where  $E$  is in eV. The energy/ToF channels, in NPD BIN mode, are logarithmically spaced ( $\Delta E = C e^x$ ;  $C = 0.44 \text{ eV}$ ;  $\Delta t = C' e^{-x/2}$ ;  $C' = 1300 \text{ ns}$ ). We calculate the energy spectrum by dividing  $N$  (expressed by Eq. (3)) by the energy channel size  $\Delta E$

$$\begin{aligned} F(t) &= \frac{N}{\Delta E} = \frac{A e^{((x-p)^2/2\sigma^2)}}{C e^x} = \frac{A}{C} e^{((x^2-2px+p^2-2\sigma^2x)/2\sigma^2)} \\ &= \frac{A}{C} e^{((x^2-2x(p-\sigma^2)+p^2)/2\sigma^2)} = A' e^{((x-p')^2/2\sigma^2)}, \end{aligned} \quad (4)$$

$$p' = p - \sigma^2; \quad A' = \frac{A}{C} e^{-p+\sigma^2/2}. \quad (5)$$

Hence, the Gaussian function (3) remains a Gaussian function after normalizing by  $\Delta E$ . For  $\Delta t$ , the formula (5)

can be obtained in a similar way:

$$p' = \frac{p + \sigma^2}{2}; \quad A' = \frac{A}{C} e^{p/2 + \sigma^2/8}. \quad (6)$$

## References

- Acuna, M.H., et al., 1998. Magnetic field and plasma observations at Mars: initial results of the Mars global surveyor mission. *Science* 279, 1676.
- Barabash, S., et al., 2004. ASPERA-3: analyser of space plasmas and energetic ions for Mars Express. In: Wilson, A. (Ed.), *Mars Express: The Scientific Payload*, vol. SP-1240. p. 121.
- Futaana, Y., et al., 2006a. First observation of ENA emissions from the Martian upper atmosphere. *Icarus* 182, 424.
- Futaana, Y., et al., 2006b. Subsolar ENA jet at Mars. *Icarus* 182, 413.
- Galli, A., et al., 2006. Energetic hydrogen and oxygen atoms at the nightside of Mars. *Space Sci. Rev.*, in press.
- Galli, A., et al., 2007. The hydrogen exospheric density profile measured with ASPERA-3/NPD. *Space Sci. Rev.*, in press.
- Grigoriev, A., Barabash, S., Fedorov, A., 2003. MarsExpress ASPERA-3 NPD FM2 Calibration Report. March 18.
- Grigoriev, A., Futaana, Y., Barabash, S., Fedorov, A., 2007. Observations of the Martian subsolar ENA jet oscillations. *Space Sci. Rev.* 126, 1–4.
- Holmström, M., Barabash, S., Kallio, E., 2002. Energetic neutral atoms at Mars: I. imaging of solar wind protons. *J. Geophys. Res.* 107 (A10), 1277.
- Kallio, E., 1996. An empirical model of the solar wind flow around Mars. *J. Geophys. Res.* 101, 11133.
- Kallio, E., Luhmann, J.G., Barabash, S., 1997. Charge exchange near Mars, the solar wind absorption and energetic neutral atom production. *J. Geophys. Res.* 102, 22183.
- Krasnopolsky, V.A., Gladstone, G.R., 1996. Helium on Mars: EUVE and PHOBOS data and implications for Mars' evolution. *J. Geophys. Res.* 101, 11765.
- Lundin, R., et al., 2004. Solar wind-induced atmospheric erosion at Mars: first results from ASPERA-3 on Mars express. *Science* 305, 1933.
- Mura, A., Milillo, A., Orsini, S., Kallio, E., Barabash, S., 2002. Energetic neutral atoms at Mars: 2. Imaging of the solar wind–Phobos interaction. *J. Geophys. Res.* 107 (A10), 1278.
- Roelof, E.C., Williams, D.J., 1988. The terrestrial ring current: from in situ measurement to global images using energetic neutral atoms. *John Hopkins APL Techn. Dig.* 9, 144.